ISSN 8755-6839

SCIENCE OF **TSUNAMI HAZARDS**

Journal of Tsunami Society International

Volume 35 **Number 3** **2016**

BATHYMETRIC SOUNDING by REMOTE SENSING

Using ELECTROMAGNETIC RADIATION

Frank C Lin[1,*], George Pararas-Carayannis [1], Piyarat Silapasuphakornwong[2]

[1]Tsunami Society International, Honolulu, Hawaii 96815, USA
[2]Human Media Research Center, Kanagawa Institute of Technology, Kanagawa 243-0292, Japan

ABSTRACT

We describe a novel *modus operandi* to survey the ocean floor. We utilize the eruption of submarine volcanoes as a light source. The electromagnetic radiation emitted by such eruptions illuminate the ocean floor and thus provides information about the barythmetric topology, and a geostationary satellite can monitor this. Since the wavelength of the electromagnetic radiation is many orders of magnitude shorter than that of the acoustic wave, finer details of the bathymetric features can be obtained. We show that a topographical representation of the seabed can be derived from the Signal Diagram by a simple transformation (a mirror reflection). In this case the radiation is emitted by water molecules stimulated by the heat of the volcanic eruption, in contradistinction to the case of tsunami radiation, where the water molecules are stimulated by mutual collisions at high speed. We give two examples: Illapel, Chile and Chichi-shima, Japan. We have also shown that water molecules in the ocean, when stimulated by the heat of submarine volcanic eruption, will emit infrared radiation

Keywords: *Tsunami Radiation, Signal Diagram, Remote Sensing, Infrared Topography, Illapel, Chile, Chichi-Shima, Japan.*

**Corresponding author: linbfrank@gmail.com Tel/Fax: 662 612 4705*

1. INTRODUCTION

The deepest part of the ocean is to a large extent still *terra incognita*. Ocean relief originates from tectonic, erosional, depositional and volcanic processes. We can identify four major divisions on the ocean floor—(a) the continental shelf, (b) the continental slope, (c) the continental rise, (d) the abyssal plain. Besides these, there are many associated features—ridges, hills, seamounts, guyots, trenches, canyons, sleeps, fracture zones, island arcs, atolls, coral reefs, submerged volcanoes and sea-scarps. A knowledge of the ocean topography is of economic interest; for example, for fisheries, mineral extraction and potential source of oil. There is DNA evidence that life on earth began at hot ocean vents at the bottom of the ocean. Along the eastern and western rims of the Pacific a deep trench demarcates the subduction of tectonic plates. The morphology of oceans influences navigation, fishing, mining, climate, exploration and other important activities of man.

At present, bathymetric sounding is mainly performed by using sonic pulses. There are two types of sonars, active or passive. In active sonars, the transducer emits an acoustic signal, which bounces off an object, and this echo when received will determine the range of the object. This principle is the same as radar using radio waves. Passive sonars do not emit signals; they only receive noise from submerged sources such as submarines, whales and ships. The frequencies of the sonar signals can be as high as 1Mhz to provide higher resolution, or as low as 50kHz - which has a low resolution but is able to travel further distances.

In this paper we propose a novel methodology to sound the ocean depth, utilizing the fact that electromagnetic radiation, mostly in the infrared part of the spectrum, emitted by erupting submerged volcanoes or vents, will illuminate the ocean floor much as a flashlight will illuminate a dark room. This radiation is captured by a geostationary satellite, the analysis of which will yield topographical information, which is not available otherwise. The use of electromagnetic waves has the advantage, *vis-à-vis* sonic waves: it travels at the speed of light, its wavelength is many orders of magnitude shorter, and it is far more energetic. It can propagate in water, in atmosphere, and in vacuum. The record of such events is permanently stored and retrievable in satellite image archives. Although such events are limited to periodic eruptions, this is not a serious drawback since portions of the ocean floor where such events do not occur are static.

1. THE 16 SEPTEMBER 2015, ILLAPEL, CHILE EARTHQUAKE AND TSUNAMI

The Peru-Chile Trench is the active boundary of collision of the Nazca Plate with the South American Plate. Subduction of the Nazca plate beneath the South America continent is not homogeneous. As a result, asperities and structural complications have caused segmentation along the entire margin, resulting in zones with different rates of slip, seismic activity, volcanism, uplift, terracing and orogenic processes (Pararas-Carayannis, 2010). The northern upper end of the central seismic zone from 33º-30ºS is delineated by the oblique subduction of the leading edge of the Juan Fernández ridge with the Peru-Chile Trench near Valparaiso and the appearance of volcanism at the

southern end (Fig. 1) Five tsunamigenic earthquakes have occurred in this area in historic times: November 19, 1811; November 19, 1822; October 16, 1868; August 17, 1906 and March 3, 1985 (Pararas-Carayannis, 2010).

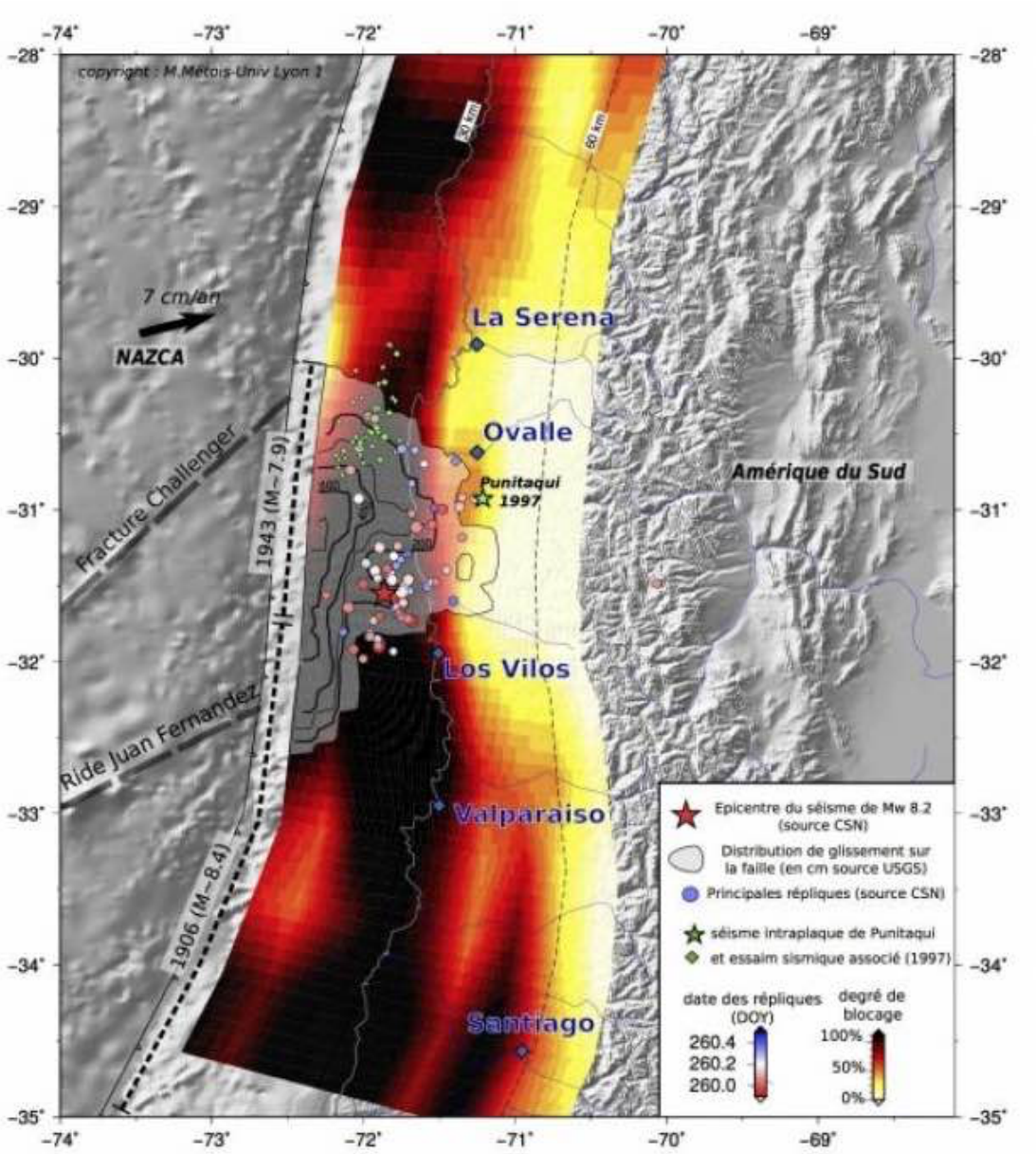

Fig. 1. Slip model of the earthquake and the aftershocks. The black areas are very locked areas or areas accumulating stress and capable of generating massive earthquakes (image via @cppgeophysics) http://earthquake-report.com/wp-content/uploads/2015/09/Screen-Shot-2015-09-19-at-11.59.55.jpg

On September 16, 2015 at a distance of 46 km from Illapel, Chile, and at 22:54:33 hours UTC, an earthquake with a moment magnitude of 8.3 occurred along the northern central zone bounded by the Juan Fernandez Ridge to the south and the Challenger Fracture to the north (Fig. 1). The initial quake lasted three minutes, and was followed by several aftershocks greater than magnitude six. The earthquake occurred on thrust faults along the boundary of the Nazca and South American plates. [1] The depth of the epicenter, located at 31.57˚ S and 71.65˚ W, was 22.4 km. At the latitude of this event, the Nazca plate is moving towards east-northeast at a velocity of 74 mm/yr. with respect to South America, and begins its subduction beneath the continent at the Peru-Chile Trench, 85 km to the west of the September 16 Earthquake (see Figs. 1 and 2). The size, location, depth and mechanism of this event are all consistent with its occurrence on the megathrust interface in this region. The length times the width of the event is about 230x100 km, or more concisely, an area of 23,000 sq. km. By comparison, the distance from Illapel to Santiago is approximately 230 km. [Lin et al 2016].

In order to compare the functionality of the electromagnetic sounding paradigm and other methods such as multibeam echo sounding or satellite radar deep-sea topography, we present in the following three figures to visually illustrate the pros and cons of our method *vis-à-vis* the conventional approach. We emphasize that there is a fundamental distinction since the conventional approach and our method are measuring different physical quantities. In the former case it is the actual seafloor being measured, and in the latter case the heat intensity being reflected into space.

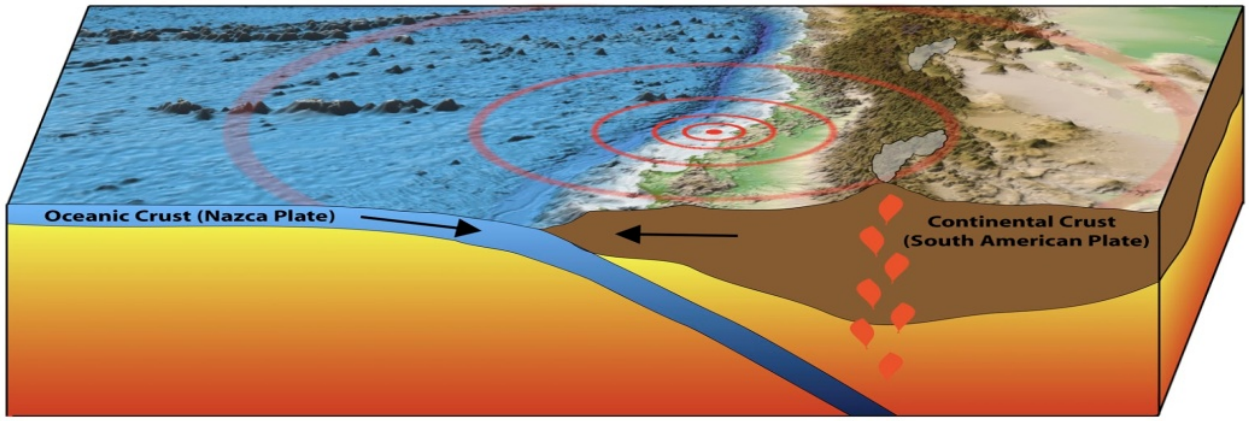

Fig. 2: Illapel Seaquake and the Peru-Chile Trench

In Fig. 2 we show an artist's version of the event, where the concentric circles radiate outward from the epic center. In the drawing we are able to discern the relative locations of the Pacific Ocean, the Peru-Chile Trench, the coastline of the South American continent, and the Andes mountain [3].

Figure 3, below shows the topographic features of the Chile Trench [4]:

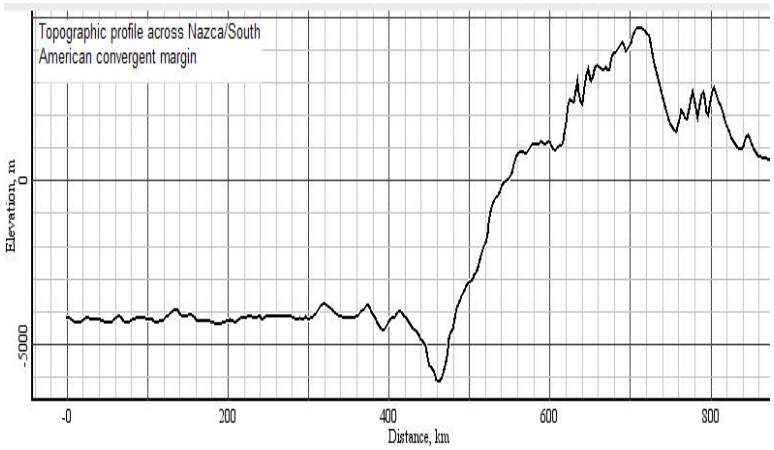

Fig. 3: Topographic profile across the Nazca-South American Plates

Here we recognize the same locations as in the artist's version, but this is a topographic representation of the seafloor relief. It shows that the seafloor steadily rises towards the South American continent and culminates in the peak of the Andes Mountain.

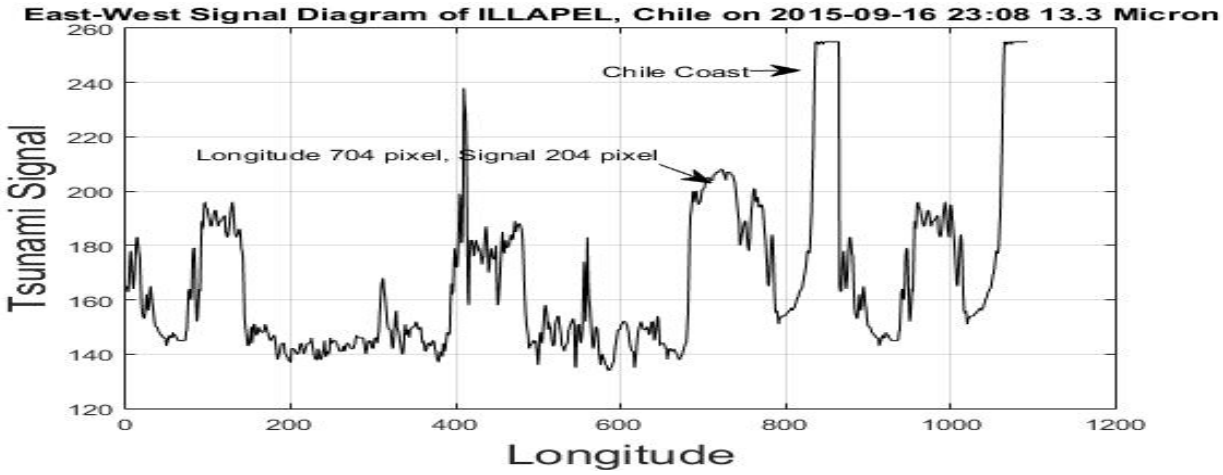

Fig. 4: Latitudinal Signal Diagram on 2015-09-16 at 23:08 UTC for 13.3 μm

In Fig. 4 we show a Signal Diagram [Lin et al, 2016], which represents a slice across the satellite image along the latitude of the seaquake event. Referring to the x-axis of Fig. 4, we note that the Tsunami Signal (which is the pixel brightness of the satellite image) at longitude 704 pixels is very broad, extending approximately 25 pixels in width (corresponding to a terrestrial distance of about 100 km); In this figure the Chilean coastline is clearly delineated, as pointed to by an arrow. We can also observe the enhanced radiation on the subduction zone from pixel 400 up to pixel 700 (i.e. the Continental Shelf) as compared with the Pacific Ocean for pixels less than 400. A very strong

peak at longitude 400 pixels demarcates the Peru- Chilean trench.

In comparison to the topographic relief map of Fig. 3., we are able to discern many 'fine structures', which indicate the existence of 'hot spots' such as erupting volcanoes, seamount vents, and fractures in the seabed. The sharp spike at 400 pixels indicates that a vast amount of heat has evolved due to the subduction of the Nazca plate below the South American plate. The seaquake itself, located at approximately 700 pixels, is remarkably extensive in size as compared to other submarine seismic events. A minor fracture appeared at about 550 pixels, and there appear to exist another hot spot in the Pacific Ocean at about 100 pixels. This interpretation is confirmed by the Signal Diagrams at the other frequencies that we have considered (3.9 μm, 6.5 μm and 10.7 μm) [Lin et al, 2016].

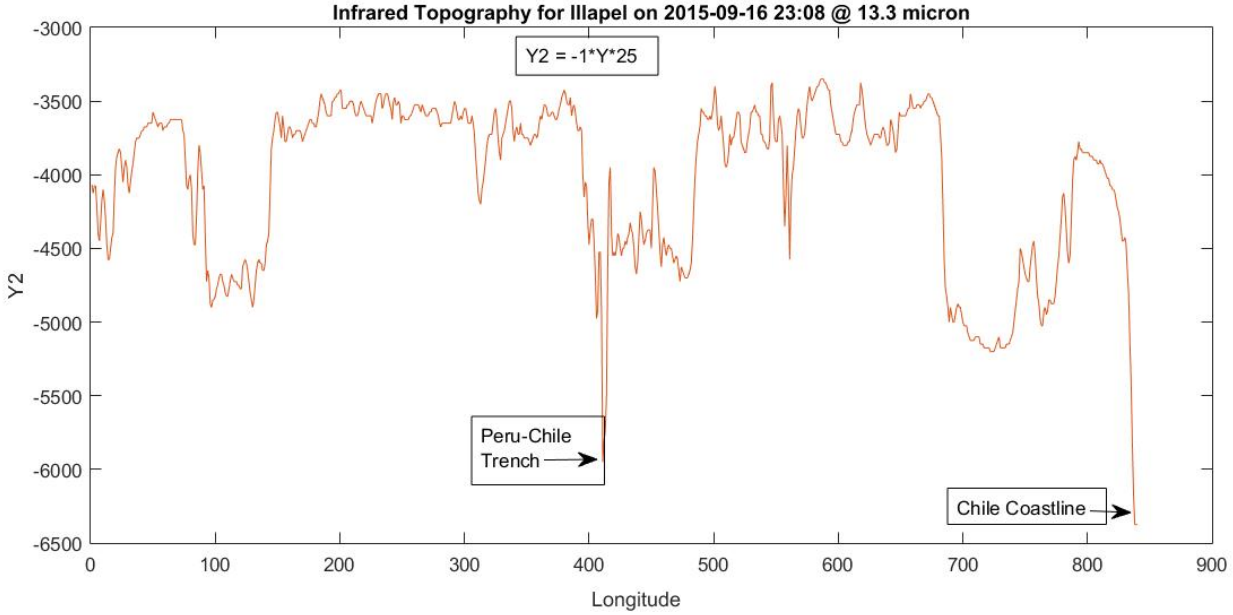

Fig. 5: Topographical Representation of Seabed at Illapel in Infrared Space

In Fig. 5 we show a topographical relief map in infrared space taken by the satellite on 2015-09-16 at 23:08 UTC, which is just 43 seconds after the eruption took place. This map is obtained by applying the following transformation (a mirror reflection) to the Signal Diagram:

$$Y2 = -1 * Y * \theta \qquad (1)$$

where Y is the Signal strength in pixels (Fig 3),
Y2 is the elevation in meters (Fig. 2)
and θ is a scaling factor (=25 in this case).

This transformation is possible since the elevation, or depth, is inversely correlated with the

temperature or heat content. The deeper the probe into the mantle, the higher is the temperature. While Fig. 3 depicts the physical feature of the terrain, Fig. 5 yields information on the *thermal* energy emitted. We emphasize, however, that the water molecules are stimulated by the heat of the volcanic eruption, in contradistinction to the case of tsunami radiation, where the water molecules are stimulated by mutual collisions at high speed. They, and not the volcanic output, give off this radiation.

We note that, in comparing Fig. 3 with Fig. 5, both figures exhibit the same gross topological features such as the Peru-Chile trench and the Chilean coastline, but the former was measured by sonic waves, whereas the latter was measured by electromagnetic radiation.

2. THE 30 MAY 2015 CHICHI-SHIMA EARTHQUAKE

On 30 May 2015 at 11:23 UTC a magnitude 7.8 seaquake with a deep focal depth of 664 km occurred WNW of Chichi-Shima, Japan at the latitude 27.8˚ N and 140.9˚ E. It centered in the vicinity of Torishima, which is a strategic location of considerable interest to geologists, since it is situated at the bisection point of the Izu-Ogasawara arc (Fig. 6).

The seaquake occurred within the interior of the Pacific plate, which subducts beneath Japan begginning at the Izu trench, a region marked by active volcanism. At this latitude, the Pacific plate moves westwards with respect to the Philippine Sea plate at the rate of 39 mm/yr. Structurally, the southern segment of the arc is underlain by thin crust of approximately 15 km on average, whereas the northern segment of the arc is underlain by an approximately 35 km thick crust. Andesitic magmas dominate volcanic eruptive products from the former and mostly basaltic lavas erupt from the latter. Where the crust is thin, melting occurs at relatively low pressures in the mantle wedge producing andesitic magmas. Where the crust is thick, the melting pressures are higher and only basaltic magmas tend to be produced. Since soon after subduction was initiated on earth most crust was thin, the rate of continental crust accumulation, which is andesitic in composition, would have been greatest. [Tamura et al, 2016].

The Izu-Ogasawara arc is produced by subduction of the Pacific plate beneath the Philippines Sea Plate. The subduction zone is characterized by rapid plate convergence and high-level seismicity extending to depth of over 600 km. It extends from 35˚N near Tokyo to 24˚N, the northern end of the Mariana arc. All volcanoes along the southern segment, except Sofigan and Nishinoshima, are submarine. We are, however, able to illuminate submarine features using electromagnetic radiation accompanying volcanic eruptions.

In Fig. 6 we show artist's version of the physical features of Japan [5], and in Fig. 7 the physical relief by sonic measurements. The Izu-Ogasawara arc is visible in Fig. 6 at approximately 140˚ longitude.

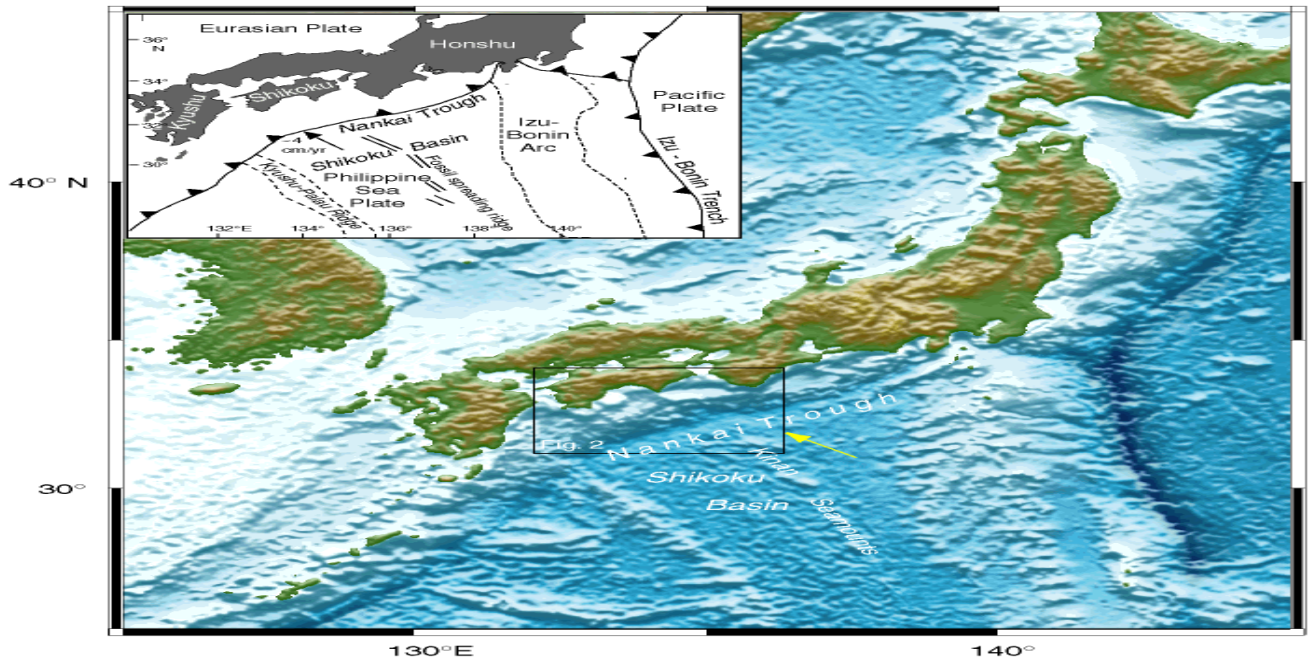

Fig. 6: Physical Features Map of Japan

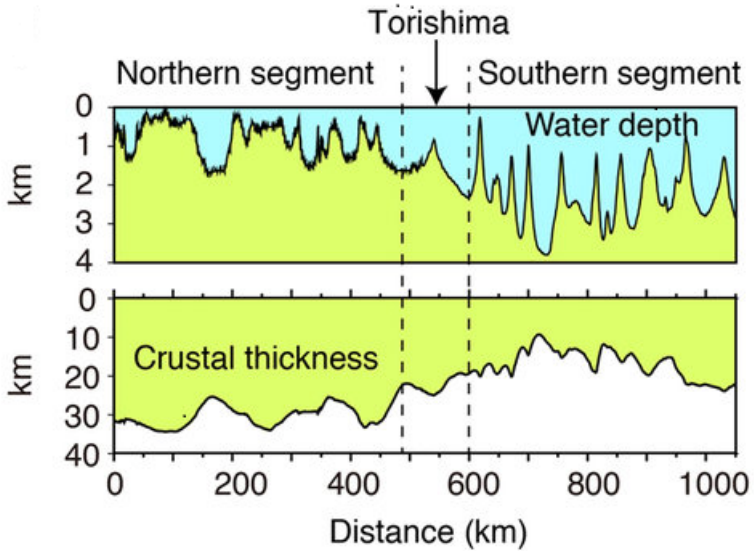

Fig. 7: Submarine Topology and Crustal Thickness at Tonishima

The Izu-Ogasawara arc is situated between a large depression, called the Shikoku Basin to the west, and the Japan Trench to the East. We shall show these features in the Infrared Topography derived from photographs obtained by the MTSAT-2 geostationary satellite at the time of the volcanic eruption. The satellite image shown below (Fig. 8) was obtained by the Japanese geostationary satellite MTSAT-2 on 2015-05-30 11:32 UTC at 10.8 μm wavelength [2].

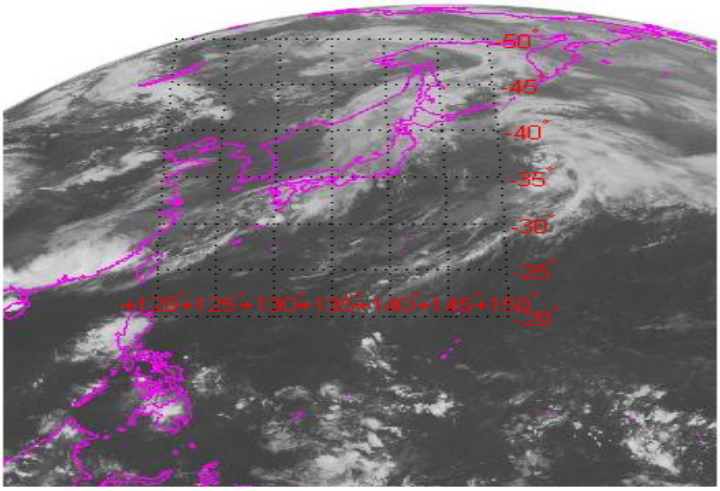

Fig. 8: Chichi-Shima Satellite image at 2015-05-30 11:32 UTC @10.8μm

The exposure is made 9 minutes after the occurrence of the volcanic eruption. At 10.8 μm, this is the long wavelength or IR-C (also classified as IR-4) band [Lin et al 2010; Lin and Sookhanaphibarn 2011; Lin et al. 2011; Lin et al. 2012; Lin et al. 2013; Lin et al. 2014]. The IR photon energy is between 0.001 and 1.7 eV. This is the atmospheric window covered by detectors such as HgCdTe and microbolometers. Satellite images in this frequency region can be used to determine cloud heights and types, to calculate land and surface water temperatures, and to locate ocean surface features. These infrared pictures are also used to depict ocean eddies or vortices and map currents. This infrared electromagnetic radiation resulted from the transition of the water molecules from the vibrational-rotational level (7 4 4) to the ground state (0 0 0). Quantum mechanically this corresponds to a [R L1 L2] (rotation, liberation) configuration conversion [Lin et al 2011; Lin et al 2012; Lin et al 2015; Lin et al 2015; Lin et al 2016]. Sulphur compounds, such as S-H or S-S, or Silicon compounds, such as Si-H or $Si-O_2$, that may be present in the volcanic output, do not emit photons at this frequency, which corresponds to a wave number of 925 cm^{-1}.

In order to be able to locate the epicenter on the satellite image we superimposed a geodetic grid onto the satellite image. The result is shown in Fig. 8. The algorithm to accomplish this is shown in Fig. 9.. We used the Robinson projection for the overlay. The Robinson projection is neither conformal nor equal-area, but is defined by a table at 5 degree intervals. It stretches the poles into long lines instead of leaving them as points. The straight parallels imply severe angular distortion at the high latitudes toward the outer edges of the map, a fault inherent in any pseudo cylindrical projection. Consequently, since distances are not conserved, it is possible that errors may be introduced. We attempt to minimize this error by choosing reference points as close as possible to each other, with the epicenter within the extent of these reference points, such as using two arbitrary points A and B with A:(30.145) degrees, or (296,193) pixels, and B:(25,135) degrees, or (242,225) pixels.

```
I = imread('chi-chi 2015-05-30 11_32 L=27.8 LN=140.5.jpg');
latlim = [-20 -50];
lonlim = [120 150];
figure, imshow(I);
axesm('Robinson','MapLatLimit',latlim,'MapLonLimit',lonlim,...
    'Scalefactor',[390],'falseeasting', [289],'falsenorthing',[356],...
    'Frame','on','Grid','on',...
    'mlinelocation', [5], 'mlinevisible','on',...
    'plinelocation',[5], 'plinevisible', 'on',...
    'mlabellocation',[5],'meridianlabel','on',...
    'plabellocation', [5],'parallellabel','on',...
    'fontcolor',[1 0 0],  'labelformat', 'signed',...
    'MLabelParallel', 'north','glinestyle', ':','PLabelMeridian','east',...
    'MeridianLabel','on','ParallelLabel','on')
%
```

Fig. 9: Algorithm to overlay geodetic lines on satellite image

By applying the MATLAB software as described in the Appendix of Ref. [Lin et al 2016] using the satellite image of Fig.8 as input, we obtain the East West Signal Diagram shown below (Fig. 10):

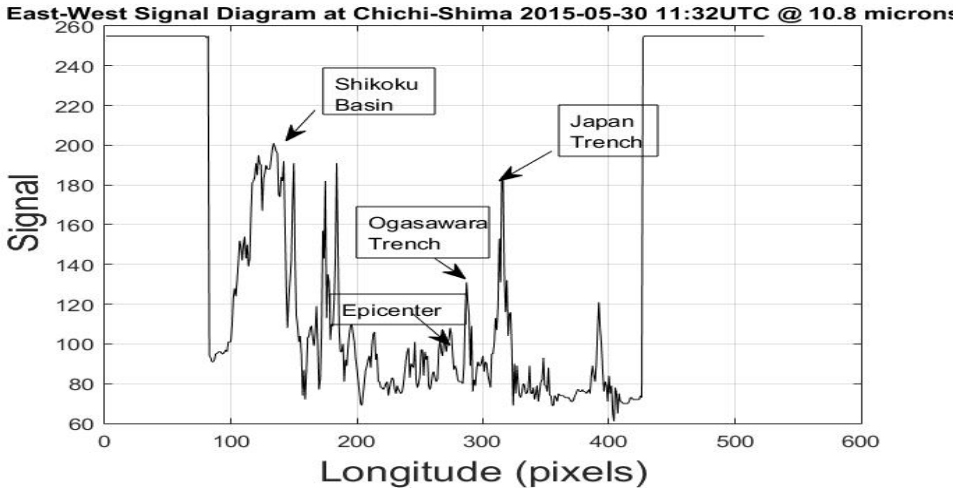

Fig. 10: Signal Diagram at Chichi-Shima 2015-05-30-11:32UTC @10.8μm

This Signal Diagram represents a slice across the satellite image in the East-West direction at the epicenter of the seaquake. The Signal on the y-coordinate is the pixel brightness. The spikes, therefore, represent the relative intensity of the infrared radiation emitted by water molecules at the corresponding locations. Since the Signal Diagram is not intuitively accessible to interpretation, we have, as before, converted it into the Infrared Topography.

At the boundary of subduction of the tectonic plates, a vast amount of heat is generated resulting in prominent spikes or jigged plateaus, some of which we have identified in the Infrared Topography, shown in Fig. 11 below, which is obtained by applying Eq. (1) to the Signal Diagram while setting the scaling constant to θ=0.1.

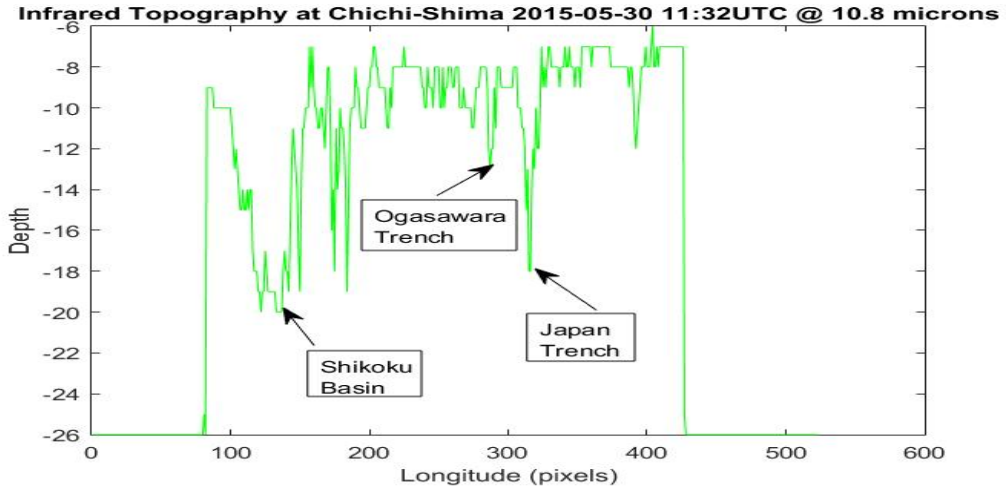

Fig. 11: Infrared Topography of Chichi-Shima, Japan

It is instructive to compare the Infrared Topography, Fig.10, with the Physical Topography, Fig.6. While both exhibit the same gross features, there are considerable differences, as to be expected.

The electromagnetic wave as a probing medium is capable of 'seeing' many 'fine structure', such as seamounts and thermal vents, as we have mentioned earlier. A thorough survey of the entire ocean will furnish us with detailed information on the geomorphology at active zones of the ocean both past and present.

3. CONCLUSION

In conclusion, in the case of Illapel, Fig2 is the physical relief obtained by sonic measurements using a naval vehicle, whereas Fig.4 is the Infrared Topography obtained by electromagnetic radiation using a geostationary satellite. In the case of Chichi-Shima, Fig.6 is the physical relief obtained by sonic measurements using a naval vehicle, whereas Fig.10 is the Infrared Topography obtained by electromagnetic radiation using a geostationary satellite. In conjunction, both methods will give us a more complete picture of the ocean's floor.

We have also shown that water molecules in the ocean, when stimulated by the heat of submarine volcanic eruption, will emit infrared radiation.

REFERENCES

[1] https://en.wikipedia.org/wiki/2015_Illapel_earthquake. Accessed 2016./9./20

[2] http://inventory.ssec.wisc.edu/inventory/ Accessed 2016/10/20

[3]
https://www.google.co.th/search?q=peru+chile+trench+diagram&sa=X&biw=1024&bih=674&tbm=isch&imgil=vLtAkJQk5LaNuM%253A%253Bx0oZviQnlRduxM%253Bhttps%25253A%25252F%25252Fcaninoesciproject.wordpress.com%25252F2013%25252F05%25252F09%25252Fsecond-stop-peru-chile-trench%25252F&source=iu&pf=m&fir=vLtAkJQk5LaNuM%253A%252Cx0oZviQnlRduxM%252C_&usg=__VY1HCOugm5w3Qljf-_FM2r8SKCo%3D&ved=0ahUKEwjCo8eFvpvPAhUEl5QKHfUYDqwQyjcILw&ei=HOHfV8KlMYSu0gT1sbjgCg#imgdii=vLtAkJQk5LaNuM%3A%3BvLtAkJQk5LaNuM%3A%3BH1DsiT3bnjhROM%3A&imgrc=vLtAkJQk5LaNuM%3A Accessed 2016/9/19

[4]
https://www.google.co.th/search?q=ocean+bottom+relief,+chile&biw=1024&bih=674&tbm=isch&imgil=XnCxNYPdY1kOwM%253A%253Bs01lr10WhhoM7M%253Bhttps%25253A%25252F%25252Fopentextbc.ca%25252Fgeology%25252Fchapter%25252F18-1-the-topography-of-the-sea-floor%25252F&source=iu&pf=m&fir=XnCxNYPdY1kOwM%253A%252Cs01lr10WhhoM7M%252C_&usg=__zeYR-MLDEVHsIrliLUYn_jBCoyo%3D&ved=0ahUKEwjMpIyTvZvPAhURtJQKHSKCCMYQyjcIIw&ei=LODfV8zeLpHo0gSihKKwDA#imgrc=jcxb8qdbEyxjSM%3A . Accessed 2016/9/20

[5]
https://www.google.co.th/search?q=ocean+bottom+relief,+japan&biw=1024&bih=710&tbm=isch&tbo=u&source=univ&sa=X&ved=0ahUKEwi-5-bK25jPAhXFm5QKHRFzAFEQsAQIHw#imgrc= wvGsBSZ6lsXfSM%3A .accessed on 2016/9/19

[6] Lin F.C., K. Na Nakornphanom, K. Sookhanaphibarn, and C. Lursinsap, 2010. "A New Paradigm for Detecting Tsunamis by Remote Sensing"; International Journal of Geoinformatics, Vol.6, No.1, March 2010, pp.19-30.

[7] Lin F.C. and K. Sookhanaphibarn, 2011. "Representation of Tsunamis in Generalized Hyperspace" Proceedings of the IEEE International Geoscience and Remote Sensing Symposium (IGARSS'11), Sendai/Vancouver, July 21, 2011. pp. 4355-4358

[8] Lin. F.C., K. Sookhanaphibarn, W. Choensawat and G. Pararas-Carayannis, 2016. "Detection of Tsunami Radiation at Illapel, Chile on 2015-09-16 by Remote Sensing"; Science of Tsunami Hazards, Vol.35, No.1, p.1

[9] Lin, F.C., K. Sookhanaphibarn, V. Sa-yakanit and G. Pararas-Carayannis, 2014. "REMOTE: Reconnaissance & Monitoring of Tsunami Events"; Science of Tsunami Hazards, Vol.33, No.2, pp.86-111

[10] Lin. F.C., K. Sookhanaphibarn, G. Pararas-Carayannis, 2015. "On The Frequency Spectrum of Tsunami Radiation"; Science of Tsunami Hazards, Vol.34, No.3, p.144

[11] Lin F.C., W. Zhu and K. Sookhanaphibarn, 2011. "Observation of Tsunami Radiation at Tohoku by Remote Sensing"; Science of Tsunami Hazards, Vol.30, No.4, pp. 223-232.

[12] Lin, F.C., W. Zhu and K. Sookhanaphibarn, 2012. "A Detail Analysis of the Tohoku Tsunami by Remote Sensing"; Proceedings of the IEEE International Geoscience and Remote Sensing Symposium (IGARSS'12), Munich, Germany, pp.1166-1169.

[13] Lin. F.C., W. Zhu and K. Sookhanaphibarn and P. Silapasuphakornwong, 2013. "REMOTE:-A Satellite Based Tsunami Early Warning Detection System"; Proceedings of the IEEE International Geoscience and Remote Sensing Symposium (IGARSS' 13), Melbourne, Australia, pp. 3694-3697.

[14] Pararas-Carayannis, G., 2010."Chile Earthquake and Tsunami of 27 February, 2010 - Evaluation of Source Mechanism and of Near and Far-field Tsunami Effects", International' Journal "Science of Tsunami Hazards", Vol. 29, No. 2, (2010)

[15] Tamura Y., Sato T., Fujiwara T., Kodaira S. and Nichols A., 2016. "Advent of Continents: A New Hypotheses: Scientific Reports 6"; Article #33517, Accessed 2016/10/25. http://www.odp.tamu.edu/publications/prosp/196_prs/196f01.html